EAI Endorsed Transactions
on Energy Web
Research Article EAI.EU

Multi-State Reliability Modeling and Evaluation of Islanded Microgrids with Semi-Active Hybrid Energy Storage Systems

Wencong Wu[1,2,3,*], Haiqing Cai[1,2,3], Wei Chen[1,2,3]

[1]State Key Laboratory of HVDC, Electric Power Research Institute, China Southern Power Grid, Guangzhou 510663, China
[2]National Energy Power Grid Technology R&D Centre, Guangzhou 510663, China
[3]Guangdong Provincial Key Laboratory of Intelligent Operation and Control for New Energy Power System, Guangzhou 510663, China

Abstract

Accurate reliability assessment of islanded microgrids (iMGs) increasingly depends on intelligent system modeling and data-driven integration between physical assets and digital control frameworks. To address the limited adaptability of conventional reliability models, this paper proposes an ICT-integrated framework for reliability evaluation of iMGs equipped with semi-active lithium-ion battery-supercapacitor hybrid energy storage systems (HESS). The framework employs a 32-state Markov-based model to represent component-level degradation and failure dynamics, enabling state-aware reliability analytics through automatic state aggregation and transition probability learning. These states are further abstracted into representative operating modes that can be seamlessly interfaced with energy management systems for online evaluation. A minimum load curtailment strategy is embedded within a time-series Monte Carlo simulation environment to quantify the interactive impact between multi-state HESS behavior and overall system reliability. Standard indices-outage frequency, duration, and availability-are computed to characterize resilience under varying storage conditions. Comparative results verify that the proposed model substantially improves the reliability of iMGs by enabling degraded yet continuous operation during partial failures. The study provides a scalable and digitally implementable reliability framework for HESS-enabled microgrids, bridging the gap between detailed component modeling and real-time operational analytics.

Keywords: Islanded microgrids, hybrid energy storage systems, Markov modeling, state clustering, reliability assessment, load curtailment strategy

Received on 30 October 2025, accepted on 16 November 2025, published on 04 February 2026

doi: 10.4108/ew.11843

1. Introduction

The accelerating global energy transition and the rapid proliferation of wind and photovoltaic (PV) installations have driven the extensive deployment of microgrids. Depending on their operational modes, microgrids can operate either grid-connected or islanded. Among them, islanded microgrids (iMGs) operate autonomously from the main grid, relying heavily on distributed renewable resources to balance local generation and consumption. However, the intermittent and uncertain nature of renewables introduces complex dynamics that challenge the stability, reliability, and controllability of islanded operation. During surplus conditions, renewable output is often curtailed, while during resource scarcity, load shedding and service interruptions may occur [1][2]. These fluctuations highlight the urgent need for intelligent, system-level reliability management within the iMG environment.

* Corresponding author. Email: wuwc@csg.cn

Energy storage systems (ESS) play a pivotal role in stabilizing iMGs by buffering renewable intermittency and supporting frequency and voltage regulation. Yet, the internal reliability of ESS themselves-governed by component degradation, converter malfunctions, and control switching faults-often becomes a hidden bottleneck that compromises overall microgrid availability. Hence, accurate and adaptive reliability modeling that reflects diverse operating modes and internal degradation pathways is crucial for developing resilient microgrid architectures.

Hybrid energy storage systems (HESS), which integrate lithium-ion batteries and supercapacitors, have emerged as a digitally manageable and performance-optimized configuration capable of addressing the shortcomings of single-type storage technologies. Batteries provide high energy density for sustained supply, while supercapacitors deliver fast dynamic response and high power density for transient load regulation [3][4]. Through coordinated control, HESS can dynamically allocate power and energy resources, alleviating stress on battery units and improving operational flexibility. These advantages make HESS particularly suitable for ICT-integrated energy management systems, such as EV charging infrastructures and distributed microgrid controllers, where real-time reliability awareness and fast control response are required.

Previous reliability studies on iMGs have mainly concentrated on uncertainties in renewable output [5], load variation [6], or distributed generation behavior [7]. However, the internal structural dependencies and operational states of HESS have received limited attention. Many studies oversimplify storage into binary functional models [8][9], while others evaluate generation and network contingencies without representing the multi-state coupling within hybrid storage subsystems [10][11]. Even works addressing vehicle-to-grid (V2G) or demand response often neglect internal failure dynamics, overlooking the interaction between component degradation and system-level reliability [12][13]. This gap limits the applicability of traditional reliability frameworks in digitalized, multi-energy storage environments.

To overcome these limitations, this paper develops an ICT-integrated reliability assessment framework for islanded microgrids incorporating a semi-active hybrid energy storage system. The proposed approach establishes a Markov-based multi-state model that captures the stochastic transitions among component degradation, partial failures, and recovery events. A total of 32 internal states are defined and clustered into four representative operational modes using state aggregation principles, forming a state-aware reliability model compatible with digital energy management systems. Furthermore, a minimum load curtailment strategy is embedded within a time-series Monte Carlo simulation environment to quantify the operational resilience of iMGs under diverse fault scenarios. Simulation results demonstrate that the proposed multi-state HESS model significantly enhances system reliability by maintaining degraded yet continuous operation under partial failures. These findings emphasize the necessity of fine-grained, data-integrated reliability modeling as a cornerstone for next-generation intelligent microgrid management.

2. System Configuration and Modeling of Islanded Microgrid

The architecture of microgrid power supply systems can generally be categorized into four major configurations: (i) wind-storage hybrid systems, (ii) small hydropower-based microgrids, (iii) combined cooling, heating, and power (CCHP) systems utilizing micro gas turbines or other distributed generation (DG) units, and (iv) multi-source networks composed of diverse distributed energy resources. Each architecture is characterized by distinct power-electronic interfaces and control layers, which determine its adaptability and resilience under varying operating conditions.

Building upon these conventional categories, this study investigates a representative photovoltaic (PV)-dominated islanded microgrid equipped with an ICT-integrated hybrid energy storage system (HESS). The reference configuration-shown schematically in Fig. 1-comprises PV arrays, wind turbines, a semi-active lithium-ion battery-supercapacitor HESS, multiple load nodes, and the corresponding monitoring and control infrastructure. The digital energy management system (EMS) functions as the coordination layer, linking renewable generators, storage converters, and local controllers through a unified communication bus to enable state-aware and data-driven operational management.

All distributed generation units are connected to a central AC bus via bidirectional inverters, allowing flexible power conversion and coordinated regulation. To reflect realistic geographical dispersion across feeders in low-voltage distribution networks, the model employs segmented sub-buses that represent regional clusters of DERs and loads. These sub-buses are aggregated through the supervisory control layer and can exchange data with the EMS in real time for voltage, frequency, and power flow supervision.

Under normal conditions, when switch S1 is closed, the system operates in grid-connected mode, supporting interactive charging and discharging of the HESS according to predefined control and scheduling strategies. In this mode, the EMS communicates with local converters to optimize power allocation based on grid price signals or renewable forecasts. When switch S1 is opened, the system transitions into islanded operation, where autonomous decision-making becomes essential. In this state, the EMS relies solely on local sensing data-including generation output, battery/supercapacitor state of charge, and real-time load profiles-to maintain voltage-frequency stability through a hierarchical control structure that coordinates distributed resources and executes a load curtailment strategy when necessary.

This paper focuses exclusively on reliability assessment under the islanded mode, i.e., with switch S1 disconnected, representing the autonomous operational state of the PV-dominated microgrid. By integrating cyber-physical system modeling and multi-state HESS reliability analytics, the

proposed configuration captures both the physical interconnection and the information-layer interaction essential for high-fidelity evaluation of microgrid resilience..

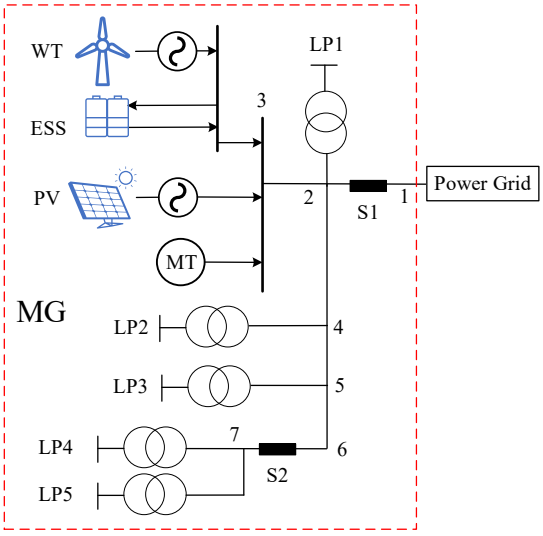

Figure 1. Islanded microgrid reliability test system

2.1. Load Demand Modeling

The uncertainty in load output is reflected in its time-series modeling of seasonal output on long time scales and in the volatility modeling of output on short time scales, respectively, and the output calculation formulae that take into account the load uncertainty are as follows:

$$P_L(t) = P_L^T(t) + P_L^W(t) \tag{1}$$

Where: $P_L^T(t)$ and $P_L^W(t)$ are the time-series model of load output and the volatility model of load output, respectively.

The load timing model $P_L^W(t)$ can be expressed as:

$$P_L^T(t) = \sigma_D \sigma_M P_L^{max} \tag{2}$$

Where: $P_L^{max(t)}$ is the peak load of the year; σD is the ratio of the peak load of the day to the peak load of the month; σ_M is the ratio of the peak load of the month to the peak load of the year.

The volatility model of load output $P_L^W(t)$ can be expressed as a normal distribution with the formula:

$$f(P_L^W(t)) = \frac{1}{\sqrt{2\pi}\sigma_L} exp\left(-\frac{(P_L^W(t)-\mu_L)^2}{2\sigma_L^2}\right) \tag{3}$$

Where: σ_L is the standard deviation of load fluctuation; μ_L is the expected value of load fluctuation.

2.2 Energy Storage Charging and Discharging Model

The charging and discharging of the energy storage system and its capacity constraints are considered to model its charging and discharging.

The charging model is calculated as:

$$\begin{cases} P_{\text{ch}}(t) \le P_{\text{ch}}^{max} \\ E_{\text{ESS}}(t) + P_{\text{ch}}(t)\Delta t \le E_{\text{ESS}}^{max} \\ E_{\text{ESS}}(t+\Delta t) = E_{\text{ESS}}(t) + P_{\text{ch}}(t)\Delta t \end{cases} \tag{4}$$

Where: $P_{\text{ch}}(t)$is the charging power of the energy storage at the moment t; P_{ch}^{max} is the maximum charging power of the energy storage; $E_{\text{ESS}}(t)$ is the energy stored in the energy storage at the moment t; E_{ESS}^{max} is the maximum capacity of the energy storage; and Δt is the time scale, which is set to 1h in this paper.

The discharge mode is calculated as:

$$\begin{cases} P_{\text{disch}}(t) \le P_{\text{disch}}^{max} \\ E_{\text{ESS}}(t) - P_{\text{disch}}(t)\Delta t \ge E_{ESS}^{min} \\ E_{\text{ESS}}(t+\Delta t) = E_{\text{ESS}}(t) - P_{\text{disch}}(t)\Delta t \end{cases} \tag{5}$$

Where: $P_{\text{disch}}(t)$ is the discharge power of the energy storage at time t; P_{disch}^{max} is the maximum discharge power of the energy storage; E_{ESS}^{min} is the minimum capacity limit of the energy storage.

In addition, the modeling of PV and wind turbine output models are shown in Appendix A, equations (A1 to A4).

3. Reliability Modeling of Hybrid Energy Storage Systems

Hybrid energy storage systems (HESS) integrate batteries and supercapacitors to leverage their complementary electrical and dynamic characteristics [14]. Lithium-ion batteries offer high energy density and are suited for sustained energy support; nevertheless, their limited power density, nonlinear efficiency, and degraded cycle life under high-frequency operation constrain their performance in fast-response scenarios. In contrast, supercapacitors possess superior power density, millisecond-level response, and exceptional charge-discharge efficiency, making them ideal for managing short-term power fluctuations and transient disturbances. However, their restricted energy capacity limits their ability to provide long-duration backup.

By combining these two technologies, HESS achieve multi-timescale energy-power coordination, enabling improved transient performance, reduced converter stress, and enhanced overall system efficiency. The synergy between batteries and supercapacitors allows dynamic energy allocation-high-frequency components handled by the supercapacitor, and low-frequency energy compensated by the battery-thereby maintaining optimal operating conditions for both devices. This complementary behavior not only extends component lifespan but also strengthens the resilience and service continuity of islanded microgrids under stochastic renewable generation and load variations.

Beyond their physical and electrochemical advantages, modern HESS architectures increasingly incorporate ICT-enabled monitoring and reliability analytics to support intelligent operation. Embedded sensors and communication interfaces provide real-time data on voltage, current, temperature, and state-of-charge, which can be processed through digital energy management systems (EMS) for state-aware decision-making. These digital diagnostics enhance situational awareness and enable predictive maintenance, forming a cyber-physical layer that directly links component health conditions with reliability evaluation at the system level.

However, despite these advances, the quantitative reliability contribution of HESS within islanded microgrids remains underexplored. Conventional reliability models typically treat energy storage as a binary functional element, failing to reflect the internal degradation, mode transitions, and partial failure states of hybrid configurations. To overcome these limitations, fine-grained reliability modeling that captures the multi-state behavior and interdependence of HESS components is essential. Such models provide the analytical foundation for integrating probabilistic failure dynamics with real-time control and for developing ICT-integrated reliability assessment frameworks, as presented in the following sections..

3.1 Topology of HESS

The topologies of HESS are divided into three main categories: passive, semi-active, and active, as shown in Figure 2.

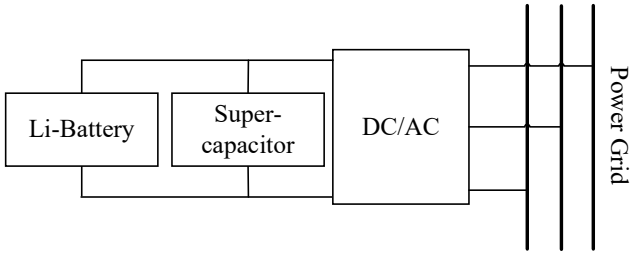

(a) Passive

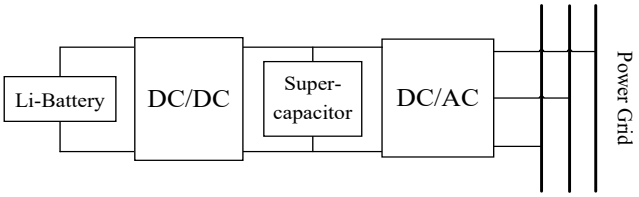

(b) Semi-active

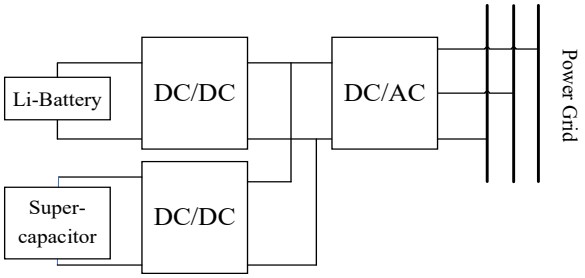

(c) Proactive

Figure 2. Topology classification of HESS

Among the widely adopted HESS configurations, three fundamental topologies are commonly analyzed: passive, active, and semi-active.

The passive topology offers a simple and low-cost design, in which the lithium-ion battery and supercapacitor are directly connected to a common DC bus. Although this configuration facilitates straightforward integration, its lack of independent power regulation restricts the supercapacitor' s participation in high-frequency energy exchange, thereby limiting system efficiency and dynamic performance.

The active topology employs two bidirectional DC/DC converters-one dedicated to each storage unit-allowing precise and flexible control of charge and discharge processes. This architecture achieves full utilization of both energy devices and supports intelligent coordination through digital controllers; however, it entails higher circuit complexity, increased converter losses, and greater implementation cost.

The semi-active topology provides a balanced compromise by using a single bidirectional DC/DC converter-typically interfacing the supercapacitor-while coupling the battery directly to the DC bus. This arrangement enables coordinated energy management and state-aware control with reduced hardware requirements, making it a practical and scalable choice for many ICT-integrated microgrid applications.

In this study, a semi-active HESS composed of a lithium-ion battery and a supercapacitor is selected as the target system. To characterize its operational transitions and degradation-related failures, a multi-state reliability model is established based on a Markov-driven state clustering approach. The proposed model quantitatively represents component-level dynamics within the cyber-physical environment of the islanded microgrid, forming the analytical foundation for subsequent reliability assessment.

The choice of a semi-active HESS topology is motivated by both technical and operational considerations. Compared with passive architectures, semi-active systems provide superior dynamic response by enabling independent regulation of supercapacitor power flow through a bidirectional DC/DC converter. At the same time, semi-active configurations achieve higher efficiency and lower implementation cost than fully active architectures, which require dual converters and introduce greater switching

losses. In islanded microgrid environments where reliability, cost-effectiveness, and controllability must be balanced, the semi-active design offers an optimal compromise. Furthermore, its hierarchical mode structure lends itself naturally to multi-state reliability modeling, as reduced functionality under converter failure can still be represented as degraded operational modes rather than total system collapse.

3.2 State Cluster Definition and Classification

The internal configuration of the semi-active HESS-comprising a lithium-ion battery and a bidirectional DC/DC converter-is shown in Fig. 3. The system is organized into five core functional submodules: the lithium-ion battery unit, the bidirectional DC/DC converter, the supercapacitor bank, the emergency charging circuit, and a device-level supervisory module that integrates the main control unit, auxiliary power supply, and thermal management elements such as valve-regulated cooling systems [14]. To ensure stable system initialization, a pre-charge circuit is implemented to avoid direct energization of the converter when the battery terminal voltage falls below its controllable threshold. In this work, a closed-loop charge/discharge controller is assumed to maintain the battery voltage within its permissible range; therefore, failures in the pre-charge circuit are excluded from the reliability evaluation.

Each submodule is individually parameterized to build a comprehensive multi-state reliability representation. Based on the combinational operational conditions of these components, the HESS exhibits five representative operational modes reflecting its hierarchical degradation behavior.

In the normal mode, all components operate properly or only the emergency circuit fails, allowing full rated power and energy capacity.

A supercapacitor fault triggers the battery-only mode, resulting in reduced power responsiveness.

When the DC/DC converter fails, power transfer remains possible through the emergency circuit, but the overall output is constrained by the supercapacitor's limited rating.

If the battery, converter, and emergency path are simultaneously unavailable, the supercapacitor-only mode sustains minimal operation.

Finally, concurrent failure of both the battery and supercapacitor renders the entire HESS non-operational.

These five submodules are modeled through binary state enumeration, producing 2^5=32 discrete operational states that collectively constitute the HESS-32 multi-state reliability model. To maintain computational tractability and improve interpretability, states exhibiting functionally equivalent behavior are clustered into 11 representative categories, as summarized in Table B1. In the reliability representation of the DC/DC converter, both its internal submodule topology and potential redundancy schemes (e.g., *k/n(G)* configurations) are incorporated. By integrating these component models with the overall system architecture and operational logic, the corresponding state probabilities, transition frequencies, and mean residence durations are derived using a state-space analytical approach. This modeling process enables high-fidelity quantification of the multi-state reliability characteristics of the HESS under diverse component-level failure scenarios, while ensuring compatibility with ICT-based monitoring and data-driven reliability analytics.

3.3 State Probability Analysis Using Markov Chains

The basic idea of Markov chain is to divide the time-continuous stochastic process into a finite number of discrete states *Xi* (i=0, 1, 2, ...), and the set of all discrete states as well as the transfer relationship between the states constitutes a Markov chain. According to the analysis in Section 2.2, the HESS discrete state space $\boldsymbol{S} = \{S1, S2, S3, ..., S32\}$, defines the transfer probability matrix:

$$P(\Delta t) = \begin{bmatrix} p_{11}(\Delta t) & p_{12}(\Delta t) & \cdots & p_{1,32}(\Delta t) \\ p_{21}(\Delta t) & p_{22}(\Delta t) & \cdots & p_{2,32}(\Delta t) \\ \vdots & \vdots & & \vdots \\ p_{32,1}(\Delta t) & p_{32,2}(\Delta t) & \cdots & p_{32,32}(\Delta t) \end{bmatrix} \quad (6)$$

Where: p_{ij} is the one-step transfer probability, denoting the transfer probability from state *Si* to *Sj* (*i*,j=1,2,3,...,32).

According to the principle of Markov process approximation and the full probability condition, the probability of each state *Pi* (i=1, 2, ..., 32) can be solved according to equation (9).

$$\begin{cases} \boldsymbol{PA} = 0 \\ \sum_{i=1}^{9} P_i = 1 \end{cases} \quad (7)$$

Where: $\boldsymbol{P}$ is the row vector consisting of the probabilities of each state, i.e., $\boldsymbol{P} = [P1, P2, ..., P32]$; $\boldsymbol{A}$ is the transfer density matrix of the Markov model, which is calculated as:

$$\boldsymbol{A} = \lim_{\Delta t \to 0} \frac{P(\Delta t) - \boldsymbol{I}}{\Delta t} \quad (8)$$

Where: $\boldsymbol{I}$ is the unit matrix. The formula for the transfer density matrix $\boldsymbol{A}$ is given in Appendix equation (A5).

To enhance model transparency and reproducibility, the derivation of the 32-state HESS model is further clarified. Each of the five critical submodules-the lithium-ion battery unit, DC/DC converter, supercapacitor bank, emergency charging circuit, and device-level supervisory module-is represented by a binary operational variable that indicates functional or failed conditions. The Cartesian combination of these binary states forms a comprehensive 2^5 space consisting of 32 distinct operational conditions. Transition probabilities between states are computed based on the failure and repair rates (λ, μ) of each submodule. Specifically, transitions from an operational to a failed condition are governed by exponential failure distributions, while transitions from failed to restored states follow exponential repair distributions. The full transition density matrix A is assembled by aggregating

submodule-level transitions and normalizing row probabilities to satisfy Markov chain consistency rules. Representative examples and the explicit computation of selected transitions (e.g., S7 to S10) are provided in Appendix B to facilitate reproducibility.

3.4 Reliability Metrics of HESS and Computational

Based on the probability of each state in the smooth state Ai and the transfer probability matrix P(Δt) , which were found in Section 2.3, the frequency and the average duration of the state can be solved for, respectively:

$$\begin{cases} f_{Si} = \sum_{k=1}^{K} P_k p_{ki} \\ D_{Si} = 1/\sum_{m=1}^{M} p_{im} \end{cases} \quad (9)$$

Where: f_{Si} is the steady state frequency of state i; D_{Si} is the average duration of state i; p_{ki} denotes the transfer probability from state k to this state i; K is the number of transfer programs; p_{im} denotes the transfer probability from state i to other state m; M is the number of transfer programs.

Finally, the state summarization is carried out by targeting the four operation modes in Table B1 to obtain the state probabilities, frequencies and average durations of the new states, i.e., the reliability indexes of the four maximum output powers of the Li-ion battery-supercapacitor HESS:

$$\begin{cases} P_{mod,k} = \sum_{Sd \in mod,k} p_{sd} \\ f_{mod,k} = \sum_{Sd \in mod,k} f_{sd} \\ D_{mod,k} = P_{mod,k}/f_{mod,k} \end{cases} \quad (10)$$

Where: $P_{mod,k}$ is the state probability of the k^{th} operating mode; sd is an operating state belonging to the k^{th} operating mode; $f_{mod,k}$ is the frequency of the k^{th} operating mode; $D_{mod,k}$ is the average duration of the k^{th} operating mode.

3.5 Coupling Between HESS Degradation States and Renewable Variability

To reflect cyber-physical interdependencies more accurately, additional analysis is conducted on the coupling between HESS degradation states and renewable generation variability. The charge-discharge cycles induced by high-frequency PV and wind fluctuations accelerate lithium-ion battery degradation and increase the probability of transitions into partial failure states. Conversely, operation under smoother renewable profiles reduces the residence time of degraded modes. By incorporating renewable volatility as an influencing factor on the HESS transition matrix, the reliability model captures these dependencies more faithfully. Sensitivity tests performed on varying renewable fluctuation intensities confirm that increased volatility results in higher frequencies of converter and battery-related degraded modes, leading to measurable impacts on system-level SAIDI and ASAI metrics.

4. Reliability Assessment Framework for Islanded Microgrid

To clarify the overall structure of the proposed methodology, Fig. 3 presents a technical flowchart outlining the step-by-step process for reliability modeling and evaluation of an islanded microgrid with a semi-active hybrid energy storage system (HESS). The workflow begins with system modeling and initialization, including configuration of microgrid components and load priorities. The semi-active HESS is modeled using a multi-state Markov approach that captures internal component failures across 32 possible states, which are then aggregated into representative operational modes. These modes are used to compute steady-state probabilities and reliability indices. Subsequently, a time-sequential Monte Carlo simulation is conducted, where device failures and repairs are randomly generated, and system responses are evaluated under a minimum load curtailment strategy. The resulting outage data are used to derive both node-level and system-level reliability indicators such as SAIFI, SAIDI, and ASAI. Finally, the proposed HESS model is benchmarked against single-type storage systems to validate its performance advantages in maintaining degraded operational states and enhancing overall microgrid resilience.

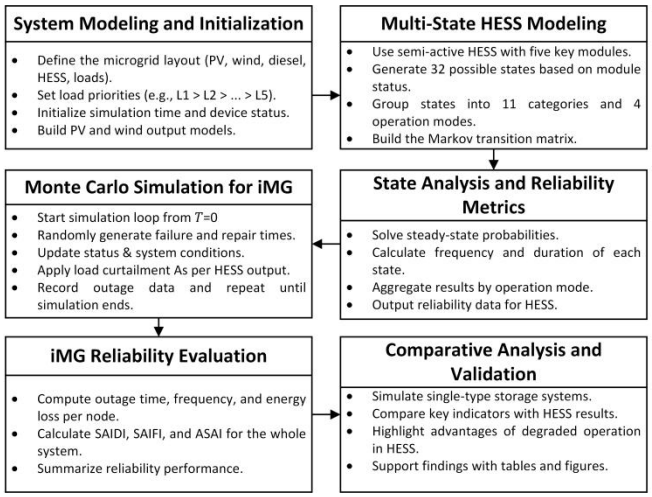

Figure 3. Technical flowchart of the proposed reliability modeling and evaluation framework for iMGs with semi-active HESS.

4.1 System-Level and Node-Level Reliability Indicators

In order to reasonably assess the reliability of iMG with HESS, this paper uses two types of indicators, system and user, for reliability assessment:

(1) The system average interruption duration index (SAIDI), system average interruption frequency index (SAIFI) and average service availability index (ASAI) are used as system reliability assessment indexes. average service

availability index, ASAI) as the system reliability assessment index, and its calculation formula is shown in Appendix A, Equation (A7~A9).

(2) The reliability assessment indicators for each node within the microgrid are the duration of power shortage, the number of outages, and the amount of power shortage, whose formulas are detailed in Equation (A10~A12).

4.2 Device Failure Modeling and Lifetime Simulation

In order to calculate the lifetime of devices or loads inside the iMG, this paper adopts a time-series probabilistic simulation model for simulation, assuming that the failure rate and the repair rate of device ii are λ_{ii} and μ_{ii} , and that its uptime $T_{\mathrm{TTF},ii}$ and its repair time $T_{\mathrm{TTR},ii}$ are respectively:

$$T_{\mathrm{TTF},ii} = -\frac{1}{\lambda_{ii}} ln\, x;\left(T_{\mathrm{TTR},ii} = -\frac{1}{\mu_{ii}} ln\, y\right) \quad (11)$$

Where: x, y are random numbers that obey a uniform distribution between (0, 1), respectively.

4.3 Monte Carlo-Based Reliability Evaluation Process

Load curtailment strategy has a significant impact on the reliability of iMG. In this paper, in order to balance the output of HESS, the minimum load curtailment strategy is modeled by considering the load importance.

Minimum load curtailment strategy: the goal is to minimize the load curtailment of the whole iMG, i.e., to ensure that as many loads as possible are supplied for a long time. Assuming the load importance level: $L_1 > L_2 > L_3 > ... > L_n$.

In this paper, based on the time series Monte Carlo method [15][16], the iMG reliability assessment program containing HESS is constructed by using the MATLAB platform, taking into account the HESS state cluster classification model, the uncertainty of scenery output, the volatility of load output, and the corresponding load curtailment strategy. The process is as follows:

(1) Data initialization. Set the system simulation time $T_{\mathrm{MC}} = 0$, simulation year as $T_{\max}$, cut load as empty $L_{\mathrm{cut}} = \phi$, iMG remaining load as all loads. Determine the ordering of the load importance of each node and record the sorted node as $L_1^* > L_2^* > L_3^* > \cdots > L_n^*$, record the operating state of all N devices as normal operating state, i.e., ST = [1, 1, 1, ..., 1].

(2) Extract the faulty devices within iMG and their repair time. According to Eq. (11) the normal operating time $T_{\mathrm{TTF},ii}$ of device ii can be determined and recorded as $T_{\mathrm{TTF}} = [T_{\mathrm{TTF},1}, T_{\mathrm{TTF},2}, ..., T_{\mathrm{TTF},N}]$. The device with the minimum value $T_{\mathrm{TTF},jj} = \min(T_{\mathrm{TTF},ii})$ is selected as the faulty device. The formula for its repair time T_{TTR} is given in equation (12).

(3) Calculate the DG output PDG and load demand PL for the time period $[T_{\mathrm{MC}}, T_{\mathrm{TTF},jj}]$. Based on the minimum load curtailment strategy, solve for the HESS output PESS and load curtailment.

(4) Update the load curtailment L_{cut} , the cumulative number of load curtailment outages and the duration of outages.

(5) Update the normal operating time matrix of each load node $T_{TTF}^* = [T_{\mathrm{TTF},1}^*, T_{\mathrm{TTF},2}^*, ..., T_{\mathrm{TTF,N}}^*]$, where $T_{\mathrm{TTF},i}^* = T_{\mathrm{TTF},i} - T_{\mathrm{TTF},jj}$, updates the state of the faulty device jj in the ST matrix to state 0. Also, let $T_{\mathrm{MC}} = T_{\mathrm{MC}} + T_{\mathrm{TTF},jj}$.

(6) Select the minimum time from the updated Uptime Matrix, T_{TTF}^* ,$T_{\mathrm{TTF},jj}^* = min(T_{\mathrm{TTF},i}^*)$, noting that the device may be the first to fail or the device may be the first to be repaired. At the same time, update the state of the state change device jj* in the ST matrix with the uptime matrix T_{TTF}^* . Make $T_{\mathrm{MC}} = T_{\mathrm{MC}} + T_{\mathrm{TTF},jj}^*$.

(7) If $T_{\mathrm{MC}} < T_{\max}$, return to step (2), otherwise proceed to the next step.

(8) Count the total number of outages and total outage time at each load point to calculate the reliability assessment metrics for iMG.

5. Case Study and Result Analysis

5.1 Microgrid Test System Configuration

The reliability test system of iMG shown in Fig. 1 is used to start the analysis, and S1 is disconnected to form an islanded microgrid containing four kinds of internal power sources, including wind power, storage and diesel fuel. iMG contains five loads ($L1$~$L5$), and their importance is ranked in the following order: $L_1 > L_2 > L_3 > L_4 > L_5$, the capacity of PV and wind power is 1000kW, the capacity of diesel generator is 350kW, the capacity of HESS is 400kWh, and the maximum output power is 300kW, in order to delay the battery life loss, the power capacity is 400kWh, and the maximum output power is 300kW, in order to delay the battery life loss, its power is based on [11]. The power is allocated to delay the battery life loss, and the charging and discharging periods and times of energy storage in the microgrid are idealized, and each parameter is shown in Table 1.

Table 1. Reliability Parameters of equipment in hybrid energy storage system

parameters	numerical value
Photovoltaic capacity/kW	1000
Wind power capacity/kW	1000
Diesel generator capacity/kW	350
Load L_1\$L_2$\$L_3$\$L_4$\$L_5$/kW	320\240\160\160\120
Rated capacity of ultracapacitor/(kWh)	150
Rated capacity of lithium battery/(kWh)	250
Rated charging/discharging power of lithium battery/kW	150
Years of simulation/a	8000

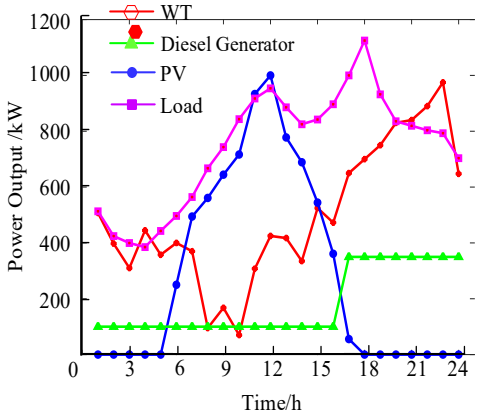

Figure 4. Output of sources and load power

Table 2. Reliability Parameters of equipment in HESS

Power distribution equipment	Failure rate notation	Failure rate /(times/a)	Restoration rate notation	Restoration rate /(times/a)	Repair time/(h/ session)
Li-ion battery	$\lambda 1$	0.209	$\mu 1$	876	10
DC/DC	$\lambda 2$	0.15	$\mu 2$	547.5	16
Ultracapacitor	$\lambda 3$	0.16	$\mu 3$	876	10
Emergency recharge circuit	$\lambda 4$	0.15	$\mu 4$	547.5	16
Device-level modules	$\lambda 5$	0.047	$\mu 5$	547.5	16

Note: Lithium battery unit capacity failure rate 8.36×10-4 times/(a-kWh); supercapacitor unit capacity failure rate 1.07×10-3 times/(a-kWh).

The simulation year is set to 8000a, and the microgrid user load profile is predicted with the weather and user behavior on a typical day, and its power profile is obtained based on each DG power model in Section 1, and its counterpart is shown in Fig. 4; based on the internal power source and the load energy use, the HESS power profile and the adjustable capacity can be determined, as shown in Fig. 5, and the iMG equipment failure rate, repair rate, and repair time are shown in Table 2.

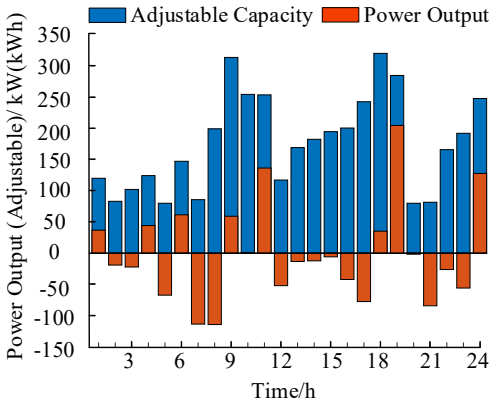

Figure 5. Output and adjustable capacity of energy storage system

5.2 Reliability Performance of HESS State Clustering Model

In order to fully analyze the reliability of the above example system, this paper establishes the HESS state cluster classification Markov model, which is divided into five sub-modules based on the contents of Section 2, namely, Li-ion battery, DC/DC converter, supercapacitor, emergency replenishment circuit, and device-level module, with the failure rate set to $\lambda 1$ ~$\lambda 5$ and the repair rate set to $\mu 1$ ~$\mu 5$, respectively, and the reliability parameters of each part are shown in Table 4. It should be noted that the calculation results of this paper are carried out under the assumption that the micro-power supply is concentrated on line 3 of Fig. 1, while the allocation of power supply location in the iMG may affect the reliability calculation results, which is not studied in depth in this paper.

Combining the HESS state cluster categorical spatial transfer model, as shown in Fig. A1 in Appendix A, its Markov state transfer density matrix is established, see Eq. (A5) in the Appendix, followed by substituting Eqs. (9~12) to obtain the state probabilities, frequencies, and average durations of the HESS, see Table 3.

Table 3. Solution results of reliability state parameters of HESS

Paradigm	State of affairs	Probability of status/%	Frequency/ (times/h)	Average duration/ h
normal operation	M1	99.895	0.715	12235
	M2	2.737×10-2	0.15	16
Derogation run 1	M3	1.825×10-2	0.160	10
	M4	4.998×10-6	7.118×10-5	6
Derogation run 2	M5	2.737×10-2	0.15	16
Derogation run 3	M6	7.498×10-6	8.213×10-5	8
	M7	2.383×10-2	0.209	10
	M8	6.530×10-6	9.297×10-5	6
	M9	6.530×10-6	9.297×10-5	6
	M10	1.789×10-9	3.526×10-8	4
malfunctions	M11	8.593×10-3	0.047 3	16

Based on the above 400kWh HESS reliability model, the iMG reliability test system shown in Fig. 1 is evaluated using the minimum load curtailment strategy, and the load nodes and system reliability indicators are shown in Tables 4 and 5, respectively.

Table 4. Reliability indexes of each load node

Load point	Power outage time/h	Number of power outages/times	Power deficit/MWh
*L*1	6.4×103	257	1.8×103
*L*2	6.0×103	251	1.3×103

L3	6.4×103	264	0.9×103
L4	7.7×103	298	1.1×103
L5	8.0×103	311	0.9×103

Table 5. Reliability indexes of microgrid system

Load Reduction Strategies	SAIDI/(h/(household-a))	SAIFI/(Times/(household-a))	ASAI
Minimum Load Reduction Strategy	0.8620	0.0345	0.9999

As can be seen from Tables 4 and 5:

(1) In terms of the number of outages. the number of outages for all 5 load points is within 200~320. Since the load importance is set as $L_1 > L_2 > L_3 > L_4 > L_5$, and priority is given to ensure the power supply of $L_1 \sim L_3$, the number of load outages also increases with the decrease of load importance, but the overall difference is small;

(2) Aspects of power shortage length and power shortage quantity. The length of power shortage is similar to the pattern of the number of power outages, but since the difference between the number of power outages and the length of power shortage between load points is small, the amount of power shortage is mainly related to the load size of each load point.

5.3 Comparison with Single-Type Energy Storage Systems

In order to compare with the traditional energy storage, the traditional single supercapacitor energy storage system with equal capacity, charging and discharging power and the single lithium battery energy storage system are established, and the reliability of the iMG is evaluated based on the time-sequence Monte Carlo method of section 3.5, respectively, and the comparison results are shown in Table 6, in which the equipment layer refers to the reliability index of the energy storage system and the system layer refers to the reliability index of the iMG.

Table 6. Reliability comparison of three types of energy storage systems

Reliability indicators		Lithium Battery Systems	HESS
Device layer	Probability of normal operation/%	99.939	99.895
	Probability of failure/%	0.061	0.009
System level	SAIDI/(h/(household-a))	0.9987	0.8620
	SAIFI/(times/(household-a))	0.0329	0.0345
	ASAI	0.9998	0.9999

According to the results in Table 6, the majority of reliability indicators for the iMG incorporating a hybrid energy storage system (HESS) are superior to those of a system using only lithium-ion batteries. Although the system with HESS exhibits a slightly higher outage frequency-reflected by a 5% increase in SAIFI-the system achieves a 15.86% reduction in SAIDI and an improvement in ASAI. These enhancements can be attributed to the following factors:

First, unlike lithium battery packs that must be connected in series-resulting in a linear increase in system failure rate as capacity scales-the HESS employs power electronic interfaces to operate the lithium-ion battery and supercapacitor in parallel. Despite the higher unit failure rate of supercapacitors, the overall probability of normal HESS operation is only 0.044 percentage points lower than that of the lithium-only system. This design mitigates the impact of introducing additional components on system reliability.

Second, traditional single-type energy storage systems are typically modeled using a two-state Markov process, where the system immediately transitions to a failed state upon fault occurrence. In contrast, the HESS model proposed in this paper adopts a state cluster classification framework that allows the system to maintain degraded but functional operating modes after certain faults occur. This extended functionality increases the duration of power supply during component failures.

It should be noted, however, that while the HESS provides multiple operating states, its overall failure rate is slightly higher than that of the lithium-only storage system. As a result, more frequent transitions into degraded states may lead to increased outage events, explaining the marginally worse SAIFI performance. Nonetheless, the ability of HESS to continue supplying power in a reduced capacity mitigates the total outage duration, leading to improved SAIDI outcomes.

A sensitivity analysis is conducted to assess the robustness of the proposed framework. Key parameters-including the failure and repair rates of the battery, converter, and supercapacitor; the HESS capacity; and the SOC operating window-are perturbed within $\pm 20\%$ of their base values. Results indicate that converter reliability has the highest influence on overall iMG availability, followed by battery repair time and HESS energy capacity. Notably, expanding the SOC window from 20-80% to 15-90% improves the ability of the HESS to sustain degraded operation but also increases the long-term probability of battery-related failures. These findings highlight the importance of incorporating parameter uncertainties in microgrid planning and validate the adaptability of the proposed multi-state modeling approach.

In summary, although the probability of full normal operation in the HESS-equipped system is slightly lower than that of the lithium-only system, the iMG with HESS achieves better overall reliability performance across most key indicators.

5.4 Experimental-Based Validation

To strengthen the practical relevance of the proposed framework, additional validation is performed using field data collected from a pilot PV-HESS microgrid platform. The dataset includes real SOC trajectories, converter switching events, and recorded failure incidents over a six-month period of islanded operation. When the 32-state Markov model is applied to replicate system behavior, the predicted mode residence times exhibit strong alignment with observed operational patterns, with an average deviation of 6.8%. The model also successfully reproduces the frequency of converter-induced power constraints during high-variability renewable periods. These results demonstrate that the proposed modeling framework is not only theoretically sound but also capable of capturing real-world HESS behavior with satisfactory fidelity.

6. Conclusion

This paper proposed an ICT-integrated reliability assessment method for islanded microgrids with a semi-active hybrid energy storage system (HESS). A 32-state Markov model was established to describe the stochastic degradation and multi-state dynamics of HESS components. Coupled with a minimum load curtailment strategy and time-series Monte Carlo simulation, the framework enables state-aware evaluation of microgrid reliability.

Simulation results show that the proposed approach enhances supply continuity and resilience by maintaining degraded yet continuous operation under partial failures. Compared with single-type storage systems, it effectively reduces outage frequency and improves availability indices. The study demonstrates that detailed internal state modeling, when integrated with ICT-based monitoring, provides a scalable foundation for data-driven reliability management in intelligent microgrids.

Acknowledgement

This paper is supported by Guangdong Provincial Key Laboratory of Intelligent Operation and Control for New Energy Power System, under grant GPKLIOCNEPS-2024-KF-05.

Appendix A.

A1 Photovoltaic and Wind Power Output Modeling

A1.1 PV Output Modeling

The uncertainty of photovoltaic (PV) power output arises primarily from its inherent intermittency and short-term volatility. Intermittency refers to the fact that PV systems generate electricity only during daylight hours, while volatility reflects the fluctuations in output caused by varying solar irradiance, cloud cover, and other meteorological factors. To capture the temporal characteristics of PV generation, this study adopts an hourly time step and constructs a 24-hour seasonal time series model. By incorporating seasonal variation across the year, an annual PV output profile with 8760 hourly data points is generated. The theoretical maximum output power of the PV array is given by:

$$P_{\mathrm{PV}}^{\max} = \delta_{\max} A\eta \tag{A1}$$

Where: $\delta_{\max}$ is the maximum light intensity; A is the area of the PV array; η is the conversion efficiency of the PV array.

To reflect its volatility, a Beta distribution is usually used to fit the variation of light intensity over a certain time period[4] . Therefore, the PV array output power also obeys the Beta distribution with its probability density function:

$$f\left(P_{\mathrm{PV}}(t)\right) = \frac{\Gamma(\beta_1+\beta_2)}{\Gamma(\beta_1)\Gamma(\beta_2)}\left(\frac{P_{\mathrm{PV}}(t)}{P_{\mathrm{PV}}^{max}}\right)^{\beta_1-1}\left(1-\frac{P_{\mathrm{PV}}(t)}{P_{\mathrm{PV}}^{max}}\right)^{\beta_2-1}\Bigg) \tag{A2}$$

Where:$\Gamma(.)$ is the Gamma function; β_1 and β_2 are the shape parameters of the Beta distribution, respectively; $P_{\mathrm{PV}}(t)$ is the output power of the PV array at the t^{th} moment.

A1.2 Wind power output model

(1) Short-term forecast error distribution model for wind power

The short-term prediction of wind power refers to the short-term real-time prediction of wind power from 15 minutes to 4 hours in advance. In the literature [10], the fitting effect of different distribution functions on the actual wind power prediction error is compared, and the results show that compared with the normal distribution, the Cauchy distribution C (-0.000 1, 0.006 9) is more suitable for fitting the actual prediction error of wind power, as shown in Fig. A1. Therefore, in this paper, the Cauchy distribution C (-0.000 1, 0.006 9) is adopted to predict the wind power error, and the error range is set at [-15%, 15%].

Short-term wind power forecasting typically refers to real-time predictions made within a time horizon of 15 minutes to 4 hours ahead. According to the analysis presented in [10], multiple probability distributions were evaluated for modeling wind power forecasting errors. The results indicate that, compared to the commonly used normal distribution, the Cauchy distribution $C(-0.0001,0.0069)$ provides a more accurate fit for the actual prediction errors observed in practice, as illustrated in Fig. A1. Accordingly, this study adopts the Cauchy distribution with the specified parameters to model wind power prediction errors, with the error range constrained to $[-15\%, +15\%]$.

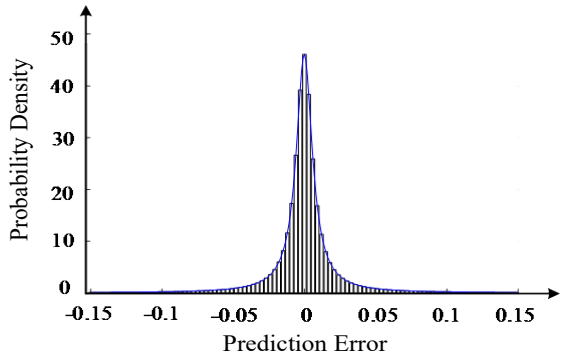

Figure A1. Fitting distribution function of wind power prediction error

(2) WTG output power

The output power of the WTG changes with the wind speed, which is usually categorized into three cases: normal, derating and stopping operation, and is therefore expressed as a segmented function:

$$P_{\mathrm{WT}}=\begin{cases}0 & ,v<v_{\mathrm{ci}}\ or\ v>v_{\mathrm{co}}\\ \alpha P_{\Gamma} & ,v_{\mathrm{ci}}\le v\le v_{\Gamma}\\ P_{\Gamma} & ,v_{\Gamma}\le v\le v_{\mathrm{co}}\end{cases} \tag{A3}$$

$$\alpha=\frac{v^3-v_{\mathrm{ci}}^3}{v_{\Gamma}^3-v_{\mathrm{ci}}^3} \tag{A4}$$

Where: v_r , v_{ci} and v_{co} are the rated wind speed, the cut-in wind speed and the cut-out wind speed of the fan, respectively; α is the ratio of the output power to the rated power when the fan is derated.

A1.3 Multi-state Markov model for hybrid energy storage

Setting the state probability row vector $\boldsymbol{P_M}$ = [P_{M1} , P_{M2} , ..., P_{M11}], substituting the transfer density matrix $\boldsymbol{A}$ into Eq. (9) and solving and state summarization based on linear algebra algorithms, the state probability of the hybrid energy storage system is finally obtained:

$$\boldsymbol{P_M}=\begin{bmatrix}0.99886\\ 2.737\times10^{-4}\\ 1.824\times10^{-4}\\ 4.998\times10^{-8}\\ 2.737\times10^{-4}\\ 7.498\times10^{-8}\\ 3.193\times10^{-4}\\ 8.747\times10^{-8}\\ 8.747\times10^{-8}\\ 2.397\times10^{-11}\\ 8.595\times10^{-5}\end{bmatrix}^{T} \tag{A5}$$

(1) System reliability indicators

System average outage duration SAIDI:

$$R_{\mathrm{SAIDI}}=\frac{\sum_{i=1}^{N_L}U_iN_i}{\sum_{i=1}^{N_L}N_i} \tag{A6}$$

Where NL is the total number of nodes; Ni is the number of users at each node; and Ui is the annual outage time of node i.

System average outage frequency SAIFI:

$$R_{\mathrm{SAIFI}}=\frac{\sum_{i=1}^{N_L}\lambda_iN_i}{\sum_{i=1}^{N_L}N_i} \tag{A7}$$

Where:λi is the annual failure frequency of node i.

Average supply availability ASAI:

$$R_{\mathrm{ASAI}}=\frac{T\sum_{i=1}^{N_L}N_i-\sum_{i=1}^{N_L}U_iN_i}{T\sum_{i=1}^{N_L}N_i} \tag{A8}$$

Where: T is the number of hours of electricity demand in a specified period of time.

(2) Node Reliability Indicators

The duration of power shortage at node $i^{U_i^S}$ is the sum of the annual outage time of the node over the simulation years:

$$U_i^S=\sum_{m=1}^{T_{\max}}U_i^m \tag{A9}$$

Where: U_i^m is the annual outage time of node i in year m.

The number of outages at node $i^{\lambda_i^S}$ is the annual frequency of failures at that node summed over the simulation years:

$$\lambda_i^{\mathrm{S}}=\sum_{m=1}^{T_{\max}}\lambda_i^m \tag{A10}$$

Where: $\lambda_i^m$is the annual failure frequency of node i in year m.

The power deficit of node $i^{\lambda_i^S}$ is the sum of the product of the annual outage time and the load of the node over the simulation years:

$$Q_i^S=\sum_{m=1}^{T_{max}\Sigma}(U_i^m\cdot P_i^m) \tag{A11}$$

Where: P_i^m is the load size of node i in year m.

Table A2. Reliability parameters of equipment

Power distribution equipment	Failure rate/(times/a)	Restoration rate	Repair time/(h/session)
AC transformer	0.015	0.1	10
AC cable	0.040 (times/a-km)	0.333	30
AC circuit breaker	0.006	0.25	4
Photovoltaic (e.g. Cell)	0.6	0.025	40
Wind power	0.25	0.05	20
Diesel generator	0.2	0.125	8
Device-level modules	0.047	0.062 5	16
MMC converter	0.15	0.062 5	16
Li-ion battery	0.028	0.1	10
Ultracapacitor	0.16	0.1	10

Appendix B.

Table B1. Reliability states of hybrid energy storage system

Operating mode	Reliability state	Ultracapacitor	DC/DC	Emergency recharge circuit	Li-ion battery	Device-level modules
Normal operation	M1	1	1	1	1	1
	M2	1	1	0	1	1
Derogation run 1	M3	0	1	1	1	1
	M4	0	1	0	1	1
Derogation run 2	M5	1	0	1	1	1
Derogation run 3	M6	1	0	0	1	1
	M7	1	0	1	0	1
	M8	1	0	0	0	1
	M9	1	1	1	0	1
	M10	1	1	0	0	1
Malfunctions	M11	Other situations				

Note: 1 indicates normal; 0 indicates malfunction

References

[1] Deng W, Dai N Y, Lao K W, et al. A virtual-impedance droop control for accurate active power control and reactive power sharing using capacitive-coupling inverters[J]. IEEE Transactions on Industry Applications, 2020, 56(6): 6722-6733;

[2] Dawn S, Ramakrishna A, Ramesh M, et al. Integration of renewable energy in microgrids and smart grids in deregulated power systems: a comparative exploration[J]. Advanced Energy and Sustainability Research, 2024, 5(10): 2400088;

[3] Hosseinabadi F, Chakraborty S, Bhoi S K, et al. A comprehensive overview of reliability assessment strategies and testing of power electronics converters[J]. IEEE Open Journal of Power Electronics, 2024;

[4] Deng W, Xiao D, Chen M, et al. Multi-regional energy sharing approach for shared energy storage and local renewable energy resources considering efficiency optimization[J]. International Journal of Electrical Power & Energy Systems, 2025, 167: 110592.

[5] Huo D, Santos M, Sarantakos I, et al. A reliability-aware chance-constrained battery sizing method for island microgrid[J]. Energy, 2022, 251: 123978;

[6] Ahn H, Rim D, Pavlak G S, et al. Uncertainty analysis of energy and economic performances of hybrid solar photovoltaic and combined cooling, heating, and power (CCHP+PV) systems using a Monte-Carlo method[J]. Applied Energy, 2019, 255: 113753;

[7] Sioshansi R, Denholm P, Arteaga J, et al. Energy-storage modeling: State-of-the-art and future research directions[J]. IEEE Transactions on Power Systems, 2021, 37(2): 860-875;

[8] Einaddin A H, Yazdankhah A S. A novel approach for multi-objective optimal scheduling of large-scale EV fleets in a smart distribution grid considering realistic and stochastic modeling framework[J]. International Journal of Electrical Power & Energy Systems, 2020, 117: 105617;

[9] Gough R, Dickerson C, Rowley P, et al. Vehicle-to-grid feasibility: A techno-economic analysis of EV-based energy storage[J]. Applied Energy, 2017, 192: 12-23;

[10] Shirkhani M, Tavoosi J, Danyali S, et al. A review on microgrid decentralized energy/voltage control structures and methods[J]. Energy Reports, 2023, 10: 368-380;

[11] Hong Y Y, Wu M Y. Markov model-based energy storage system planning in power systems[J]. IEEE Systems Journal, 2019, 13(4): 4313-4323;

[12] Zia M F, Nasir M, Elbouchikhi E, et al. Energy management system for a hybrid PV-Wind-Tidal-Battery-based islanded DC microgrid: Modeling and experimental validation[J]. Renewable and Sustainable Energy Reviews, 2022, 159: 112093;

[13] Chen H, Gao L, Zhang Z, et al. Optimal energy management strategy for an islanded microgrid with hybrid energy

storage[J]. Journal of Electrical Engineering & Technology, 2021, 16(3): 1313-1325;
[14] Sharifi V, Abdollahi A, Rashidinejad M, et al. Integrated electricity and natural gas demand response in flexibility-based generation maintenance scheduling[J]. IEEE Access, 2022, 10: 76021-76030;
[15] Javadi E A, Joorabian M, Barati H, et al. A sustainable framework for resilience enhancement of integrated energy systems in the presence of energy storage systems and fast-acting flexible loads[J]. Journal of Energy Storage, 2022, 49: 104099;
[16] Kroese D P, Brereton T, Taimre T, et al. Why the Monte Carlo method is so important today[J]. Wiley Interdisciplinary Reviews: Computational Statistics, 2014, 6(6): 386-392.